Article

n-Pentane and Isopentane in One-Dimensional Channels

Shreyas Y. Bhide, and S. Yashonath

J. Am. Chem. Soc., **2003**, 125 (24), 7425-7434• DOI: 10.1021/ja0285868 • Publication Date (Web): 21 May 2003

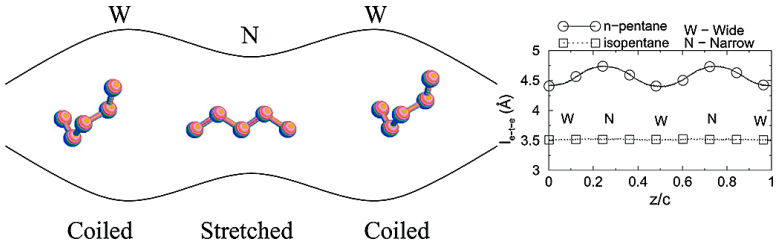

More About This Article

Additional resources and features associated with this article are available within the HTML version:

- Supporting Information
- Links to the 3 articles that cite this article, as of the time of this article download
- Access to high resolution figures
- Links to articles and content related to this article
- Copyright permission to reproduce figures and/or text from this article

View the Full Text HTML

J|A|C|S
ARTICLES
Published on Web 05/21/2003

n-Pentane and Isopentane in One-Dimensional Channels

Shreyas Y. Bhide[†] and S. Yashonath*[,†,‡,§]

Contribution from the Solid State and Structural Chemistry Unit and Supercomputer Education and Research Centre, Indian Institute of Science, Bangalore-560012, India

Received September 18, 2002; E-mail: yashonath@sscu.iisc.ernet.in

Abstract: Molecular dynamics studies of *n*-pentane and isopentane in one-dimensional channels of $AlPO_4$-5 and a carbon nanotube are reported. Variation of the structure and energetics in $AlPO_4$-5 along the channel axis of isopentane is similar to what has been found for other rigid molecular systems. In *n*-pentane, these properties exhibit more frequent undulations along the channel due to flexibility. The end-to-end distance of *n*-pentane is a function of its position along the channel in $AlPO_4$-5, suggesting that *n*-pentane has to alternately stretch in the narrow part and destretch or coil in the broader part of the channel. *n*-Pentane lies flat instead of upright on the inner surface of the carbon nanotube. Both of the species exhibit diffusive motion in $AlPO_4$-5, and the self-diffusivity is higher than that in bulk. Isopentane has a higher diffusivity than does *n*-pentane. This is attributed to the higher cross section of isopentane, which is closer to the void cross section. Further, the coupling of the translational motion with the slower dihedral angle reorientation in the case of *n*-pentane decreases its mobility. Superdiffusive motion is seen for both species in the carbon nanotube. These results can be understood in terms of the levitation effect.

1. Introduction

Confined fluids are widely encountered in many biological, chemical, and physical systems. Properties of the confined phase are often quite different from those of the bulk or the adsorbed phases.[1] This may be attributed in part to the presence of two or more surfaces surrounding the fluid. This may be contrasted with just one surface in the adsorbed phase or no surface at all in the bulk. Thus, properties of methane or *n*-alkanes adsorbed on a graphite surface are quite different when compared to those of methane or *n*-alkane in a carbon nanotube or zeolite such as silicalite. Such confined fluids are often encountered in microporous substances where the pore dimensions are in the range of 1−20 Å.[2] In contrast, the mesoporous (20−500 Å) and macroporous materials (>500 Å) have pore dimensions which are much larger than molecular dimensions, and therefore the properties of fluids confined to these substances may resemble the properties of the bulk.

In nature, there are many situations where one encounters confined fluids. Lubricating fluid which exists between two solid surfaces, hydrocarbons in zeolites encountered in petrochemical refineries, ions within a superionic conductor (e.g., AgI), or ions passing through the conduction channels in biomembranes are typical examples of the confined phase. In view of their wide prevalence, it is important to understand the basic principles that govern their properties.

In the past decade, many groups have contributed to a better understanding of the properties of confined fluids. Extensive PFG-NMR measurements of Kärger and co-workers[3] have shown that self-diffusivity exhibits surprising dependence on a number of variables such as the concentration of sorbates, nature of zeolite, temperature, etc. Detailed simulation studies of Theodorou and coworkers[4−6] have led to an increased comprehension of the relationship between microscopic details such as distribution of physisorption sites, channel geometry etc. and the transport properties. Auerbach and coworkers[7] have recently looked at the role of entropic contribution at higher temperatures. Jobic and coworkers have carried out detailed investigations into the translational motion of sorbates inside zeolites using quasi-elastic neutron scattering (QENS).[8,9]

Some of our recent studies have shown that their transport can be quite different from those of the bulk as well as the adsorbed phases. For example, for small values of the sorbate diameter, self diffusivity of the confined or sorbed fluid is found to exhibit a linear proportionality to the reciprocal of the square of the sorbate diameter. As this increases and approaches the pore dimension, a peak is found in the self diffusivity.[10]

Hydrocarbons sorbed within microporous solids such as zeolites are most commonly encountered in petroleum industries.

[†] Solid State and Structural Chemistry Unit.
[‡] Supercomputer Education and Research Centre.
[§] Also at the Condensed Matter Theory Unit, Jawaharlal Nehru Centre for Advanced Scientific Research.

(1) Klafter, J., Drake, J. M., Eds. *Molecular Dynamics in Restricted Geometries*; John Wiley: New York, 1989.
(2) Thomas, J. M. *Philos. Trans. R. Soc. London, Ser. A* **1990**, *333*, 173.
(3) Kärger, J.; Ruthven, D. M. *Diffusion in Zeolites and Other Microporous Solids*; John Wiley: New York, 1992.
(4) June, R. L.; Bell, A. T.; Theodorou, D. N. *J. Phys. Chem.* **1992**, *96*, 1051.
(5) Gergidis, L. N.; Theodorou, D. N.; Jobic, H. *J. Phys. Chem. B* **2000**, *104*, 5541.
(6) Makrodimitris, K.; Papadopoulos, G. K.; Theodorou, D. N. *J. Phys. Chem. B* **2001**, *105*, 777.
(7) Schüring, A.; Auerbach, S. M.; Fritzsche, S.; Haberlandt, R. *J. Chem. Phys.* **2002**, *116*, 10890.
(8) Fitch, A. N.; Jobic, H.; Renouprez, A. *J. Phys. Chem.* **1986**, *90*, 1311.
(9) Goyal, R.; Fitch, A. N.; Jobic, H. *J. Phys. Chem. B* **2000**, *104*, 2878.
(10) Yashonath, S.; Santikary, P. *J. Phys. Chem.* **1994**, *98*, 6368.

10.1021/ja0285868 CCC: $25.00

The properties of confined hydrocarbons in a variety of zeolites have been invistigated in considerable detail. Barrer and coworkers have investigated many of the properties of hydrocarbons in zeolites experimentally.[11] More recently, Rees and coworkers have studied a number of hydrocarbons within zeolites.[12,13] Theodorou and co-workers have investigated the sorption and diffusion of *n*-hexane and *n*-butane as well as a mixture of *n*-butane and methane in silicalite employing techniques of computer simulation.[4,5,14] Sastre et al. have studied the effects of branching on the diffusion of heptane isomers in zeolites MCM-22, ITQ-1, and ITQ-2.[15−17] Properties of alkanes in one-dimensional channels have been studied experimentally[18−20] and through computer simulation.[21−26] Newalkar et al.[27] have obtained the heat of adsorption of *n*-pentane and isopentane in $AlPO_4$-5, while grand canonical Monte Carlo (GCMC) studies of *n*-pentane in $AlPO_4$-5 have been made by Smit and co-workers.[23] van Santen and co-workers have carried out studies on linear and branched alkanes diffusing within ZSM-5 and ZSM-22, and mordenite and ferrierite.[28] They found that linear alkanes usually have a higher self-diffusivity. The chain length dependence of self-diffusivity has been investigated by a number of groups.[28−35]

One of the major needs of petrochemical refineries is the separation of branched and linear alkanes. Zeolites are commonly used in the separation of hydrocarbons in these refineries. Therefore, an understanding of the effect of branching on the properties of alkanes is important. In this paper, we investigate the properties of *n*-pentane and isopentane in one-dimensional channel systems such as $AlPO_4$-5 and the carbon nanotube. We compare these results with the bulk phase. We report structural and dynamical properties of *n*-pentane and isopentane in one-dimensional channel systems. We investigate the effect of (i) corrugations in the channel and (ii) branching of the hydrocarbon chain on these properties. The results are compared to the experimental measurements whenever available.

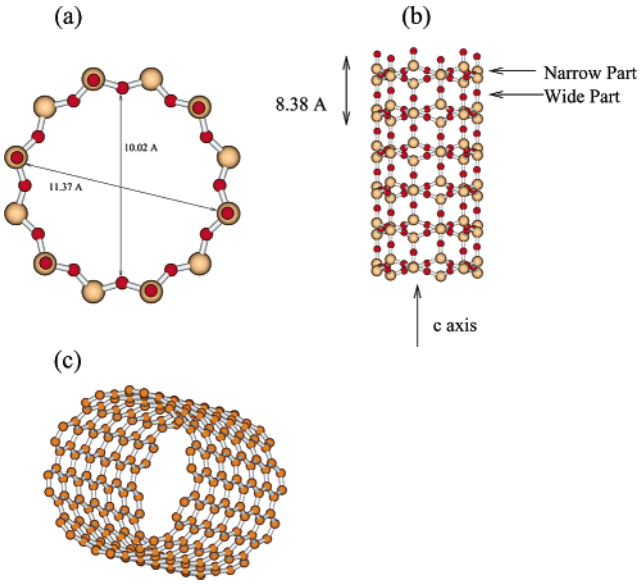

Figure 1. Schematic view of structure of different hosts used in the present study. For $AlPO_4$-5, dark spheres correspond to oxygens. (a) A cross-sectional view of the $AlPO_4$-5 channel. There are two diameters, the narrow (10.02 Å) and the broad (11.37 Å), which occur at $z = 0.25c$ and $0.5c$, respectively. (b) Vertical view of the $AlPO_4$-5 channel showing the location of narrow and wide regions. (c) Carbon nanotube.

2. Structure of Hosts

The two structures, (i) $AlPO_4$-5 and (ii) carbon nanotube, have one-dimensional channels along the *c*-axis.

$AlPO_4$-5 crystallizes in the hexagonal space group *P*6/*mcc* with $a = 13.77$ and $c = 8.38$ Å.[36] There are 72 atoms in one unit cell. The channel diameter is not uniform throughout. This can be seen from Figure 1a and b. The two values indicated (10.02 and 11.37 Å, or free diameters 7.491 and 8.841 Å, respectively) in Figure 1a (which lies in the *xy*-plane) for the cross-sectional diameter are the distance between the centers of the diagonally opposite oxygen atoms (not free diameter) at two different values of *z*. The corresponding *z* values are shown in Figure 1b: the 12-membered ring made up of 12 Al/P and 12 O's gives rise to the narrower part (diam ≈ 10.02 Å), while the six oxygens acting as a bridge between the two 12-membered rings lead to the enlarged region (diam ≈ 11.37 Å) of the $AlPO_4$-5 channel. The narrower parts of the channel are located near $z \approx 0.25c$ and $0.75c$, while the broader parts of the channel are located near $0c$ and $0.5c$.

In contrast, the carbon nanotube provides a structureless cylindrical channel. The structure of the carbon nanotube is constructed by the method of the arm-chair mode of rolling the graphite sheet[37,38] (see Figure 1c). It is possible to have carbon nanotubes with different diameters. Here we have chosen a (10,10) single walled carbon nanotube. The diameter (not free diameter, but the distance between the centers of the diagonally opposite carbon atoms) of the tube is 13.6 Å, which corresponds to a free diameter of 10.2 Å. The length of a single carbon nanotube is taken to be $c = 61.6$ Å, which contains 1000 carbon atoms. Unlike $AlPO_4$-5, the carbon nanotube has uniform diameter, and the wall is smooth and homogeneous throughout.

(11) Barrer, R. M. *Zeolites and Clay Minerals as Sorbents and Molecular Sieves*; Academic Press: New York, 1978.
(12) Hampson, J. A.; Rees, L. V. C. *J. Chem. Soc., Faraday Trans.* **1993**, *89*, 3169.
(13) Song, L.; Sun, Z.; Rees, L. V. C. *Microporous Mesoporous Mater.* **2002**, *55*, 31.
(14) June, R. L.; Bell, A. T.; Theodorou, D. N. *J. Phys. Chem.* **1990**, *94*, 1508.
(15) Sastre, G.; Catlow, C. R. A.; Corma, A. *J. Phys. Chem. B* **2002**, *106*, 956.
(16) Sastre, G.; Catlow, C. R. A.; Chica, A.; Corma, A. *J. Phys. Chem. B* **2000**, *104*, 416.
(17) Sastre, G.; Raj, N.; Catlow, C. R. A.; Roque-Malherbe, R.; Corma, A. *J. Phys. Chem. B* **1998**, *102*, 3198.
(18) Choudhary, V. R.; Mayadevi, S. *Sep. Sci. Technol.* **1993**, *28*, 2197.
(19) Jänchen, J.; Stach, H.; Uytterhoeven, L.; Mortier, W. J. *J. Phys. Chem.* **1996**, *100*, 12489.
(20) McCullen, S. B.; Reischman, P. T.; Olson, D. H. *Zeolites* **1993**, *13*, 640.
(21) Bhide, S. Y.; Yashonath, S. *J. Chem. Phys.* **2002**, *116*, 2175.
(22) Bhide, S. Y.; Yashonath, S. *J. Phys. Chem. A* **2002**, *106*, 7130.
(23) Maris, T.; Vlugt, T. J. H.; Smit, B. *J. Phys. Chem. B* **1998**, *102*, 7183.
(24) Mao, Z.; Sinnott, S. B. *J. Phys. Chem. B* **2000**, *104*, 4618.
(25) Mao, Z.; Sinnott, S. B. *J. Phys. Chem. B* **2001**, *105*, 6916.
(26) Demontis, P.; Gonzalez, J. G.; Suffritti, G. B.; Tilocca, A. *J. Am. Chem. Soc.* **2001**, *123*, 5069.
(27) Newalkar, B. L.; Jasra, R. V.; Kamath, V.; Bhat, S. G. T. *Microporous Mater.* **1997**, *11*, 195.
(28) Schuring, D.; Jansen, A. P. J.; van Santen, R. A. *J. Phys. Chem. B* **2000**, *104*, 941.
(29) Runnebaum, R. C.; Maginn, E. J. *J. Phys. Chem. B* **1997**, *101*, 6394.
(30) Tsekov, R.; Smirniotis, P. G. *J. Phys. Chem. B* **1998**, *102*, 9385.
(31) Clark, L. A.; Ye, G. T.; Gupta, A.; Hall, L. L.; Snurr, R. Q. *J. Chem. Phys.* **1999**, *111*, 1209.
(32) Goring, R. L. *J. Catal.* **1973**, *31*, 15.
(33) Nitsche, J. M.; Wei, J. *AIChE J.* **1991**, *37*, 661.
(34) Webb, E. B., III; Grest, G. S. *J. Chem. Phys.* **2002**, *116*, 6311.
(35) Webb, E. B., III; Grest, G. S.; Mondello, M. *J. Phys. Chem. B* **1999**, *103*, 4949.
(36) Richardson, J. W., Jr.; Pluth, J. J.; Smith, J. V. *Acta Crystallogr.* **1987**, *C43*, 1469.
(37) Ayappa, K. G. *Langmuir* **1998**, *14*, 880.
(38) Zhang, F. *J. Chem. Phys.* **1999**, *111*, 9082.

Table 1. Lennard-Jones Potential Parameters

type of interaction	σ (Å)	ϵ (kJ/mol)
CH_3-CH_3 (C_2)	3.905	0.7322
CH_3-CH_3 (C_3)	3.775	0.6694
CH_2-CH_2	3.905	0.4937
CH−CH	3.85	0.3347
$AlPO_4$-5		
O−O	2.529	1.51
carbon nanotube		
C_n-C_n	3.4	0.2328

Thus, these one-dimensional channels represent structures with different degrees of undulations in channel diameters and differences in surface roughness and homogeneity of the channel walls.

3. Intermolecular and Intramolecular Potential

Both *n*-pentane and isopentane are modeled using a five site model and torsional potentials. The two molecules are therefore flexible, unlike those in previous studies.[21,22,39]

Intermolecular interactions between isomers of pentane as well as between pentane isomers and zeolite are modeled using the Lennard-Jones form

$$U_{ij}(r_{ij}) = -\frac{A_{ij}}{r_{ij}^6} + \frac{B_{ij}}{r_{ij}^{12}} \qquad (1)$$

The potential parameters $A_{ij} = 4\epsilon_{ij}\sigma_{ij}^6$ and $B_{ij} = 4\epsilon_{ij}\sigma_{ij}^{12}$ for the sorbate−sorbate interaction are taken from Jorgensen et al.[40] In this model, a CH_3 or a CH_2 group is represented by a single site located at the carbon atom position within the molecule. The parameters for sorbate−host interactions have been obtained from the Lorentz−Berthelot combination rules. The interaction parameters of host atoms have been taken from earlier work,[21,22,41] and these are listed in Table 1. Here C_2 and C_3 refer to a carbon attached to a secondary or tertiary carbon atom. For more details, see Jorgensen et al.[40] Both of the isomers are assumed to interact only with oxygen atoms and not with the Al or P atoms of $AlPO_4$-5. We have chosen the C−C parameters of Steele[42] for the carbon nanotube, which are also listed in Table 1 along with the guest−guest interaction parameters.

Dihedral angle rotation of *n*-pentane occurs around C(2)−C(3) as well as C(3)−C(4) bonds, while in isopentane it is around C(2)−C(3) (see Figure 2). The potential of Jorgensen et al.[40] has been used for dihedral angle rotation:

$$U(\phi) = \sum_{n=0}^{3} c_n \cos^n(\phi) \qquad (2)$$

Parameters c_n are given in Table 2. A nonbonded Lennard-Jones interaction is included for *n*-pentane between the two CH_3 groups situated at the end. Figure 2a and b shows *n*-pentane and isopentane at a dihedral angle of $\phi = 180°$.

4. Computational Details

All molecular dynamics (MD) simulations have been carried out in the microcanonical ensemble (NVE), with cubic periodic boundary conditions. The system consists of 16×16×6 unit cells in the case of $AlPO_4$-5. There are in all 256 channels along the *c*-direction with each

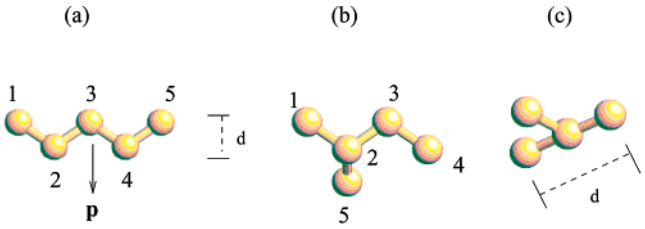

Figure 2. (a) *n*-Pentane and (b) isopentane in united atom model. *d* denotes the cross-sectional diameter in the plane perpendicular to the end-to-end vector in *n*-pentane. In (c), isopentane is drawn with the $CH-CH_2$ bond perpendicular to the plane of the paper. The projection is on a plane that is perpendicular to the $CH-CH_2$ bond for isopentane.

Table 2. Parameters for Intramolecular Potential in kJ/mol

	c_0	c_1	c_2	c_3
n-pentane	8.397288	−16.786208	1.133864	26.31736
isopentane	9.54998	24.86342	−2.230072	−28.894704

Table 3. Average Temperature of Pentane Isomers, $\langle T \rangle$, in K

	n-pentane	isopentane
$AlPO_4$-5	194.5	202.5
carbon nanotube	202.4	205.3
bulk	187.9	203.1

channel 6 unit cells long. In the case of the carbon nanotube, 256 tubes are arranged in a hexagonal fashion with all tubes parallel to the *c*-direction. In the plane perpendicular to the *c*-axis, two channel centers are separated by a distance of 17 Å. There is one molecule per channel which corresponds to a total of 256 molecules, corresponding to a concentration of 0.167 molecules per unit cell (0.0238 gm/cm^3) in $AlPO_4$-5 and 0.046 gm/cm^3 (one molecule per nanotube channel, of 61.3 Å length) in the carbon nanotube. Molecules located in neighboring channels may interact with each other. However, the sorbate−host interaction is dominant. A spherical cutoff radius, r_c, measured from the center of mass of a molecule for both sorbate−sorbate and sorbate−host interactions of 12 Å for $AlPO_4$-5 and 15 Å for the carbon nanotube has been used. Bulk MD simulations of *n*-pentane and isopentane are carried out for 108 molecules at a density of 0.634 gm/cm^3 with a cutoff radius of 12 Å. The liquid densities of these two isomers at 298 K are, respectively, 0.621 and 0.615 gm/cm^3.

Equations of motion have been integrated using the RATTLE algorithm of constraint MD.[43] The host structure is kept rigid. A time step of 1 fs has been used. A conservation of the order of 1 in 10^4 in total energy has been obtained. Different properties are calculated using positions and velocities stored at every 50 fs. The system is equilibrated for 200 ps in each case. At the beginning of the equilibration phase, pentane isomers are put at the center of the channel with initial velocities chosen randomly from a uniform distribution. The initial conformation as shown in Figure 2 is assigned with its long axis parallel to the channel axis. Initial equilibration is followed by a production run of 1 ns. As already mentioned, molecules of pentane in different channels interact with each other through the Lennard-Jones potential, and this aids in the thermalization of the system. We verified that the system is indeed thermalized well by calculating the probability distribution of the three components of the center of mass velocity. Initially, the velocity distributions were significantly different from the Gaussian distribution. However, after equilibration, we found that the distributions of all three components have identical widths corresponding to the temperature of the ensemble. In bulk MD, the system is equilibrated for 50 ps, and the production phase is 500 ps. The average temperatures obtained from the MD runs are listed in Table 3.

For *n*-pentane and isopentane, the bond length, *l*, between the two groups is taken to be 1.53 Å. The bond angle is taken to be 112°

(39) Bhide, S. Y.; Yashonath, S. *J. Phys. Chem. B* **2000**, *104*, 11977.
(40) Jorgensen, W. L.; Madura, J. D.; Swenson, C. J. *J. Am. Chem. Soc.* **1984**, *106*, 6638.
(41) Bandyopadhyay, S.; Yashonath, S. *J. Phys. Chem.* **1995**, *99*, 4286.
(42) Steele, W. A. *Surf. Sci.* **1973**, *36*, 317.
(43) Andersen, H. C. *J. Comput. Phys.* **1983**, *52*, 24.

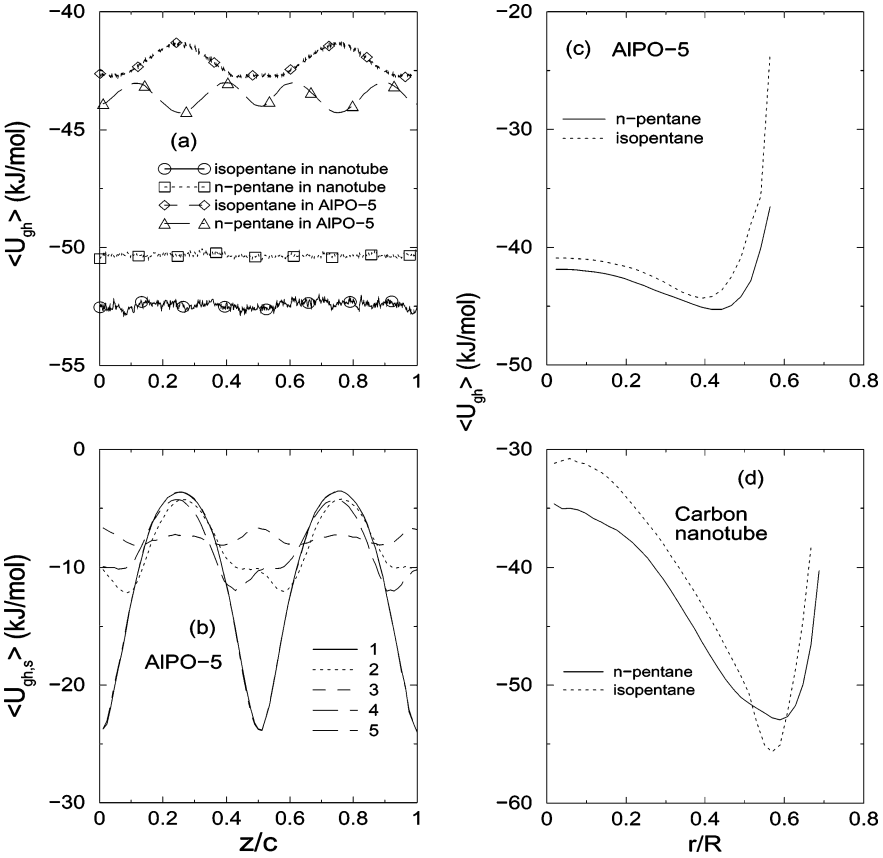

Figure 3. (a) $\langle U_{gh} \rangle$ of pentane isomers as a function of the *z* coordinate of their center of mass at $T = 200$ K. *z* is scaled by unit cell length *c* for $AlPO_4$-5 and by $c = 61.6$ Å for the carbon nanotube. The symbols are drawn at a few points along different curves to distinguish between them. (b) $\langle U_{gh,s} \rangle$, the average potential energy for each interacting group in *n*-pentane in $AlPO_4$-5. *z* is the position of a group along the channel scaled by the unit cell length *c*. (c) and (d) $\langle U_{gh} \rangle$ of pentane isomers in $AlPO_4$-5 and the carbon nanotube, respectively, as a function of *r*, the perpendicular distance of the center of mass of an isomer from the channel axis ($T = 200$ K).

following Jorgensen et al.[40] Masses of CH_3, CH_2, and CH groups are taken to be 15.034, 14.026, and 13.018 amu, respectively.

5. Results and Discussion

In previous studies, we investigated the translational and rotational dynamics of a series of small molecules confined to one-dimensional channels such as $AlPO_4$-5 and the carbon nanotube.[21,22,39] The molecules − benzene, methane, ethane − are all rigid, and they differ in size, shape, and mass. They are all rigid molecules. In the present study, *n*-pentane and isopentane have been chosen, which are linear and branched molecules, respectively. They differ in size and shape but have the same mass. In contrast to the earlier studies, these molecules are flexible and can perform dihedral angle rotation around the C−C bond. Here we study the effect of flexibility and branching on the equilibrium and dynamical properties.

5.1. Energetics and Structure. The average sorbate−host interaction energy $\langle U_{gh} \rangle$ of pentane isomers varies with the position along as well as across the channel. Figure 3a shows the variation of $\langle U_{gh} \rangle$ with *z*, the position of the center of mass of the pentane isomer. $\langle U_{gh} \rangle$ versus *z* in $AlPO_4$-5 has corrugations, while it is constant in the carbon nanotube. This arises from the fact that the channel diameter in $AlPO_4$-5 shows undulations, while the nanotube has a constant diameter with *smooth* and *homogeneous* walls. Surprisingly, the corrugations of $\langle U_{gh} \rangle$ in $AlPO_4$-5 are different for the two isomers, *n*-pentane and isopentane. The undulations in $\langle U_{gh} \rangle$ for isopentane have a wavelength $\lambda = c/2$, which agrees with the undulations in the diameter of the host structure. $\langle U_{gh} \rangle$ is higher in the narrower part of the channel and lower in the wider part of the channel. This is due to the larger contribution from the repulsive part of the guest−host potential to $\langle U_{gh} \rangle$ in the narrower part of $AlPO_4$-5 than that in the wider part.

Table 4. Average Interaction Energy[a]

	$AlPO_4$-5		carbon nanotube	
	$\langle U_{gh} \rangle$	$\langle U_{gg} \rangle$	$\langle U_{gh} \rangle$	$\langle U_{gg} \rangle$
n-pentane	−43.67	−0.0003	−50.41	−0.00018
isopentane	−42.308	−0.00019	−53.3	−0.00021

[a] $\langle U_{gh} \rangle$, $\langle U_{gg} \rangle$ are in kJ/mol.

In the case of *n*-pentane, $\lambda = c/4$ (see Figure 3a). For the underlying reasons for this, Figure 3b shows the variations in $U_{gh,s}$, the guest−host interaction energy of each of the five individual sites (with the rest of the host) as a function of the position of the respective site, *z*. It is seen that the largest barrier for migration along the *c*-axis is provided by the end methyl groups. The lowest barrier is for the central CH_2 group. Note that both CH_3 and CH_2 groups have the same σ for the guest−host interaction. The difference in the ϵ parameter gives rise to the observed higher barrier. The actual barrier shown in Figure 3a is the sum of all of the five individual terms shown in Figure 3b, taking into account the precise *z* value at which they are located within the channel. In effect, the more frequent undulations are a consequence of the molecular structure and conformational flexibility of *n*-pentane.

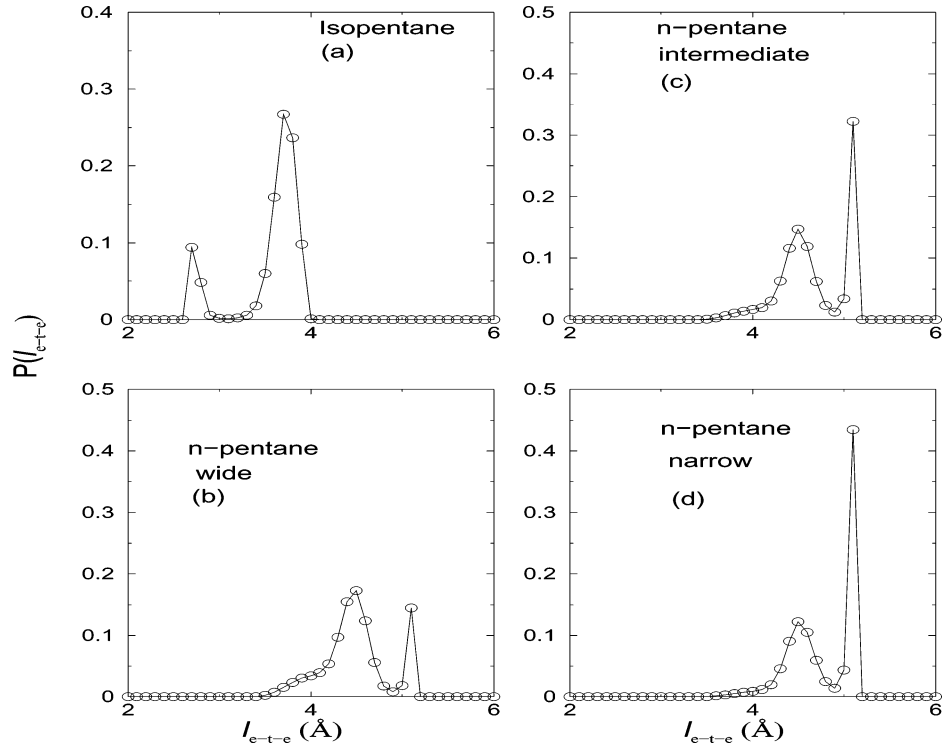

Figure 4. Probability distribution of the end-to-end distance, $P(l_{e-t-e})$ for pentane isomers in $AlPO_4$-5. (a) Isopentane in $AlPO_4$-5. (b), (c), and (d) correspond to the $P(l_{e-t-e})$ of *n*-pentane in $AlPO_4$-5 in the wide, intermediate, and narrow parts, respectively. The extent of each of these regions is as defined in the text.

$\langle U_{gh} \rangle$ as a function of radial distance r of the center of mass from the channel axis shows that for both isomers of pentane, minima occur near the channel wall (Figure 3c,d). The average interaction energies of pentane isomers in both of the channel systems are listed in Table 4. Experimentally observed values of heats of adsorption of *n*-pentane and isopentane inside $AlPO_4$-5 in the temperature range of 303−333 K at a coverage of 0.1 mmol/g are 48.32 and 53.22 kJ/mol, respectively. The present MD study is performed at a coverage of 0.114 mmol/g in $AlPO_4$-5 at 200 K. This gives heats of adsorption values for *n*-pentane and isopentane in $AlPO_4$-5 as 45.33 and 43.907 kJ/mol, respectively, using $\Delta H_{ads} = -U_{gh} + RT$, where R is the gas constant and $T = 200$ K.

The dependence of $\langle U_{gh} \rangle$ of isopentane on its center of mass position z inside of the $AlPO_4$-5 channel is similar to that observed for other rigid molecules such as benzene, ethane, and methane in $AlPO_4$-5.[21,22,39] The dependence of *n*-pentane, which is more flexible, is quite different from these. This is because of the *flexibility* of the *n*-pentane. A change in the dihedral angle is reflected in the end-to-end distance l_{e-t-e}. We have therefore looked at the end-to-end distance distribution, $P(l_{e-t-e})$, of these two pentane isomers. The end-to-end distance for *n*-pentane is measured between groups 1 and 5, while for isopentane it is measured between groups 1 and 4, see Figure 2. The static geometry of isopentane as well as the end-to-end distance distribution, $P(l_{e-t-e})$, obtained from MD (Figure 4a) indicate that l_{e-t-e} does not exceed $c/2$. Note that $c/2$ is the distance between two successive narrow or wide regions along the channel in $AlPO_4$-5. Figure 4b,c,d shows $P(l_{e-t-e})$ of *n*-pentane in different parts of the $AlPO_4$-5 channel. $P(l_{e-t-e})$ of isopentane does not show any significant change from one region to another inside the $AlPO_4$-5 channel. Therefore, $P(l_{e-t-e})$ for different regions inside $AlPO_4$-5 is not plotted. However, $P(l_{e-t-e})$ for *n*-pentane shows significant changes in narrow, wide, and intermediate regions inside $AlPO_4$-5. A molecule is considered to be in a *narrow* region if the z-coordinate of its center of mass is in the intervals $z = 0.2c - 0.3c$, $0.7c - 0.8c$, while a molecule is considered to be in a *wide* region if $z = 0 - 0.1c$, $0.4c - 0.6c$, $0.9c - 1.0c$. For other values of z, the molecule is considered to be in an *intermediate* region of the channel. Figure 4b,c,d implies that *n*-pentane is *stretched* to nearly full length in all regions of the $AlPO_4$-5 channel but with varying probability. The probability of *n*-pentane being in the *stretched* conformation increases as the molecule moves from the *wide* to *narrow* region of $AlPO_4$-5.

This behavior of isopentane and *n*-pentane is further confirmed through the calculation of the average end-to-end distance, $\langle l_{e-t-e} \rangle$, as a function of the channel length (Figure 5a). Figure 5a shows that $\langle l_{e-t-e} \rangle$ does not change for both isomers inside the carbon nanotube. In $AlPO_4$-5, $\langle l_{e-t-e} \rangle$ of isopentane remains constant throughout. However, $\langle l_{e-t-e} \rangle$ of *n*-pentane shows modulation with z, and the maxima and minima in $\langle l_{e-t-e} \rangle$ occur at *narrow* and *wide* regions of the channel, respectively. Figure 5b shows $\langle l_{e-t-e} \rangle$ as a function of the radial distance r of the center of mass of an isomer from the channel axis. For *n*-pentane, $\langle l_{e-t-e} \rangle$ is higher near the wall than the center in both of the channels. For isopentane, $\langle l_{e-t-e} \rangle$ remains almost constant from the center to the wall of a channel.

These results show that when the center of mass of *n*-pentane is in a *narrow* region of the $AlPO_4$-5 channel, it is most of the time in a *stretched* conformation. In this conformation, CH_3 groups at the end are in the wider region where the attractive part of the interaction potential dominates. When the center of mass of *n*-pentane is in a *wide* part of the channel, the end groups are in the *narrow* region of the channel where the repulsive interaction dominates (see Figures 3 and 4). These

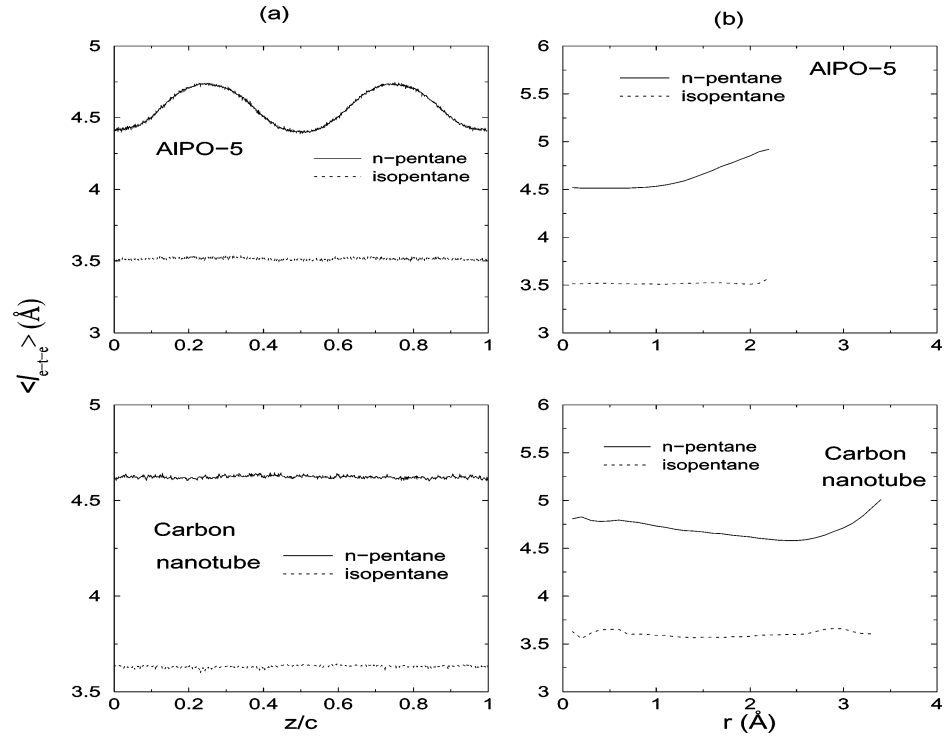

Figure 5. (a) Average end-to-end distance of pentane isomers $\langle l_{e-t-e} \rangle$, as a function of the position of the center of mass of an isomer inside $AlPO_4$-5 and the carbon nanotube. (b) $\langle l_{e-t-e} \rangle$ as a function of r, the distance of the center of mass of a pentane isomer from the axis of a channel in $AlPO_4$-5 and the carbon nanotube.

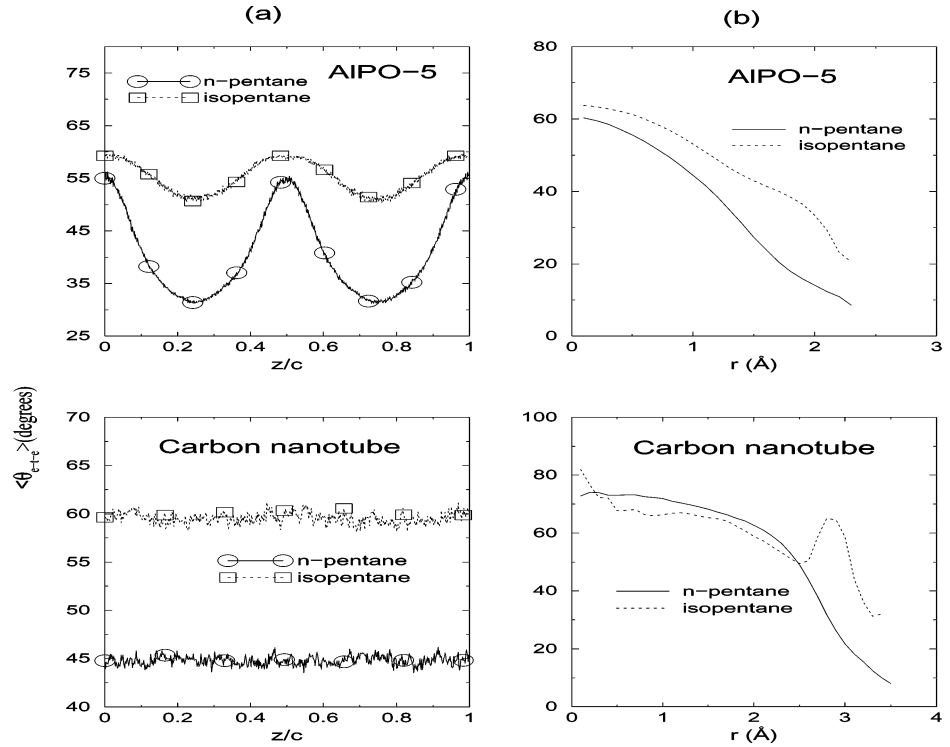

Figure 6. (a) $\langle \theta_{e-t-e} \rangle$, angle made by the end-to-end vector as a function of the position of the center of mass of a pentane isomer along the channel in $AlPO_4$-5 and the carbon nanotube. z is scaled by the unit cell length in $AlPO_4$-5 and by 61.6 Å in the carbon nanotube. (b) $\langle \theta_{e-t-e} \rangle$ as a function of r, the distance of the center of mass of a pentane isomer from the channel axis in $AlPO_4$-5 and the carbon nanotube.

conformations of *n*-pentane in $AlPO_4$-5 have been observed in grand canonical Monte Carlo studies of Smit and co-workers.[23] This gives rise to the modulation in $\langle U_{gh} \rangle$ as plotted in Figure 3a.

The structure of isomers inside the channels can also be characterized by the angle that the end-to-end vector makes with respect to the channel axis, θ_{e-t-e}. Figure 6a shows $\langle \theta_{e-t-e} \rangle$ as a function of z. Inside the carbon nanotube, the average orientation $\langle \theta_{e-t-e} \rangle$ remains constant along the channel for both pentane isomers. Inside $AlPO_4$-5, however, $\langle \theta_{e-t-e} \rangle$ shows modulations along the channel. For *n*-pentane, $\langle \theta_{e-t-e} \rangle$ changes more than isopentane as the molecule goes from the *narrow* to

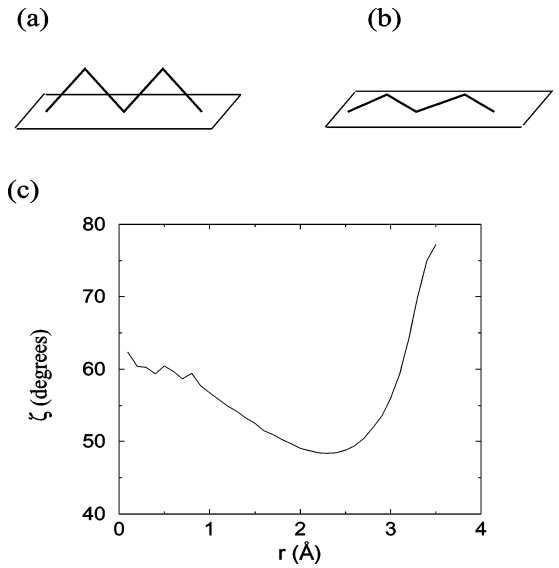

Figure 7. Schematic of the (a) standing orientation and (b) flat orientation of *n*-pentane. (c) Angle ζ made by a vector **p** (see the text for the definition of **p**) with the radial vector from the center of mass of *n*-pentane to the channel axis as a function of *r*.

wide region. The end-to-end vector of *n*-pentane is more parallel to the channel axis in the *narrow* region than in the *wide* region. Figure 6b shows the variation in $\langle\theta_{e-t-e}\rangle$ as a function of the distance of the center of mass from the channel axis. In both of the channel systems, the pentane isomers are more parallel to the channel axis near the channel wall.

There are two different orientations that the *n*-pentane molecule can assume over the inner surface of the carbon nanotube. It is possible to speak of the two orientations in the case of the carbon nanotube because its surface is *smooth* with a constant diameter: one where the molecule lies on the surface with all atoms nearly equidistant from the inner surface (flat orientation) and the other (standing orientation) where three of the atoms (C1,C3,C5) (or the two atoms: C2,C4) of *n*-pentane are closer to the surface than the other two (the other three: C1,C3,C5), as shown schematically in Figure 7a and b. A vector **p** which is in the plane of atoms 2, 3, and 4 of *n*-pentane and is the bisector of the angle C2−C3−C4 (see Figure 2a) is useful in determining whether *n*-pentane is flat or in a standing orientation. The angle that the vector **p** makes with the radial vector (the vector from the center of mass to the nearest point on the channel axis) is ζ. When $\zeta = 90°$, *n*-pentane is flat, and when $\zeta = 0°$, it is in a standing orientation. Figure 7c shows a plot of the variation of the angle ζ as a function of *r*. The average angle made by **p** is closer to 90° near the channel wall. This implies that *n*-pentane is lying flat on the surface of nanotube. At higher temperatures, there may be a larger number that are in the standing orientation.

Figure 8 shows the average distance of the center of mass of a pentane isomer, $\langle r\rangle$, from the channel axis as a function of its *z*-coordinate value. In the carbon nanotube, both pentane isomers maintain a constant average distance from the axis of the tube, although isopentane is closer to the wall than is *n*-pentane. In $AlPO_4$-5, the *n*-pentane center of mass moves closer to the channel wall in *narrow* regions than in *wide* regions where *n*-pentane remains near the center of the channel. The center of mass of isopentane in $AlPO_4$-5 remains closer to the channel axis in all regions.

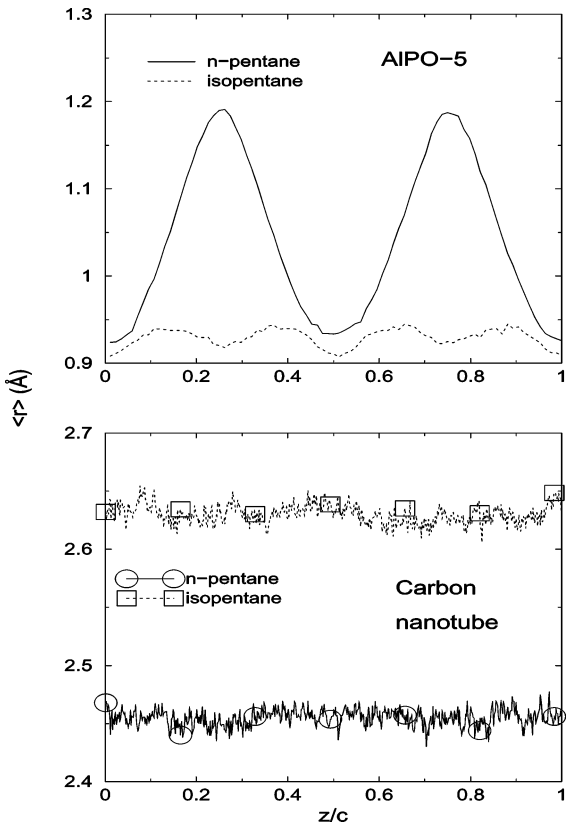

Figure 8. The average radial distance of the centers of mass of pentane isomers $\langle r\rangle$ from the channel axis as a function of the position of the centers of mass of pentane isomers along the channel in $AlPO_4$-5 and the carbon nanotube. Symbols are drawn only to distinguish between the curves.

5.2. Dynamical Properties. Translational Motion. Figure 9 shows the mean squared displacement (msd) of both pentane isomers in $AlPO_4$-5, carbon nanotube, and bulk. $\langle u^2(t)\rangle$ is linear in *t* in $AlPO_4$-5 and bulk liquid. In the carbon nanotube, $\langle u^2(t)\rangle$ does not go over to the diffusive regime. For pentane isomers in the carbon nanotube, the exponent α in $\langle u^2(t)\rangle \approx t^\alpha$ obtained from the log−log plot is 1.95 and 1.935 for *n*-pentane and isopentane, respectively. This value is closer to ballistic motion ($\alpha = 2$) than diffusive motion ($\alpha = 1$). Molecular motion along the *z*-direction in the nanotube, unlike in $AlPO_4$-5, is along an almost uniform potential energy surface along the channel (see Figure 3), which leads to nearly free particlelike motion. When this is coupled with nonballistic motion along radial directions, one obtains a value between 1 and 2 for the exponent α. At higher loadings, the motion of pentane isomers can become diffusive. In a simulation where the framework of the carbon nanotube is flexible, the randomness associated with the sorbate motion is expected to increase. This can lead to a lower value of exponent α, but the trends seen in Figure 9 remain unchanged.[44] More detailed investigations of motion within the carbon nanotube of monatomic sorbates suggest that the chaotic (diffusive) motion is interspersed with regular (ballistic) motion, leading to superdiffusive motion ($1 < \alpha < 2$).[44] We also found that the probability distributions of the three components of the velocity obtained from the MD simulations have identical widths. This suggests that the different degrees of freedom have thermalized. The properties computed are therefore likely to be those inherent to the molecules confined to the carbon

(44) Bhide, S. Y.; Yashonath, S.; Ananthakrishna, G., submitted.

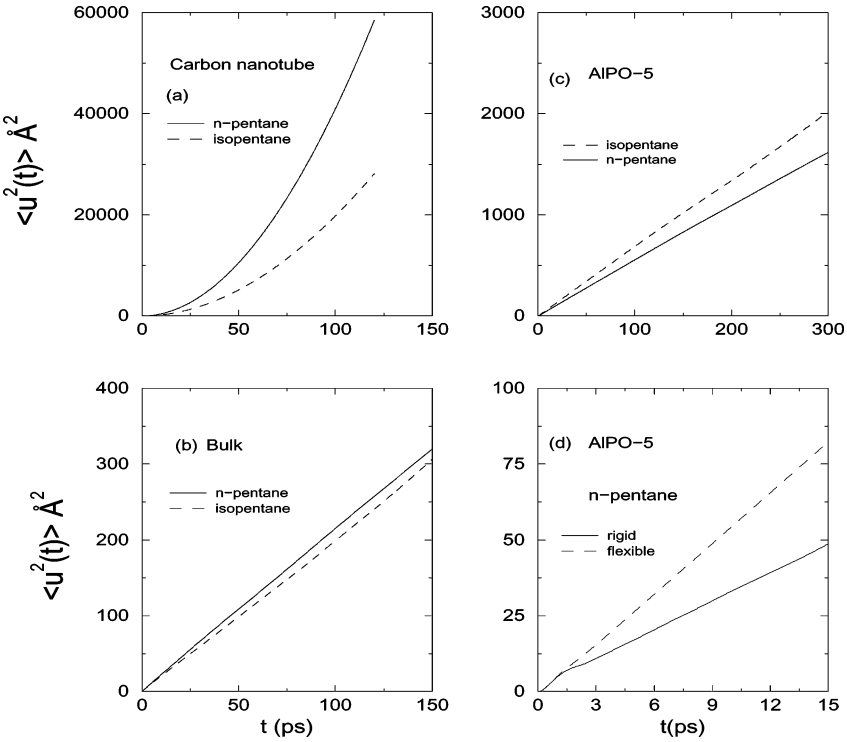

Figure 9. Mean squared displacement of the center of mass of pentane isomers (a) confined to the carbon nanotube and in (b) bulk, (c) $AlPO_4$-5, and (d) for flexible and rigid *n*-pentane at $T = 200$ K.

Table 5. Self-Diffusion Coefficient

	$D \times 10^{-8}$ m²/s	
	n-pentane	isopentane
$AlPO_4$-5	2.7	3.33
bulk	0.354	0.336

nanotubes.[44] These results at low loadings may be compared to the results of Mao and Sinnot,[24,25] who found that methane, ethane, and ethylene in the carbon nanotube exhibit diffusive and subdiffusive ($\alpha < 1$) motion at higher loadings.

The self-diffusion coefficient for pentane isomers in bulk and in $AlPO_4$-5 is obtained from Einstein's relation

$$D = \frac{\langle r^2 \rangle}{2dt} \tag{3}$$

where $d = 1, 3$ for $AlPO_4$-5 and bulk, respectively. Self-diffusivity values are listed in Table 5. These values have been obtained from the slope of the straight line fit to data in the interval 10−125 ps for bulk and in the interval 10−250 ps for $AlPO_4$-5. The error in D for *n*-pentane in $AlPO_4$-5 and in bulk is 1.5% and 3.6%, respectively. For isopentane in $AlPO_4$-5 and in bulk, the error in D is 0.7% and 1.6%, respectively.

How far do internal degrees of freedom such as dihedral angle rotation influence translational self-diffusivity? To check this, short simulations were carried out for *n*-pentane without including dihedral angle rotation in the MD integration. The molecule of *n*-pentane was assumed to be in the all-trans conformation ($\phi_1 = \phi_2 = 180°$). Figure 9d shows the evolution of the msd curve for about 15 ps. It is seen that the capability for *n*-pentane to change its conformation enables the D to enhance considerably.

As Figure 9 indicates, the mobility of pentane of the two isomers is similar in bulk, while in confinement the mobility is different for the two isomers. In $AlPO_4$-5, as described in the previous section (Figure 3), *n*-pentane experiences a more corrugated potential energy surface along the channel than that felt by isopentane. This causes isopentane to be more mobile than *n*-pentane in $AlPO_4$-5. In the carbon nanotube, both *n*-pentane and isopentane experience a potential energy that is constant along the length of the nanotube. Yet, as Figure 8 shows, isopentane is closer to the wall where it maximizes its sorbate−host interaction (Figure 3d) as compared to *n*-pentane. This increased interaction of isopentane with nanotube causes isopentane to be a bound species leading to a decreased mobility as compared to *n*-pentane.

Velocity autocorrelation functions (VACF) are plotted in Figure 10 for the centers of mass of pentane isomers in $AlPO_4$-5, carbon nanotube, and bulk. Figure 10a and d shows that, in $AlPO_4$-5, the VACF for the *z*-component of velocity decays to zero without showing any negative minimum. This is in contrast with earlier studies involving methane, ethane, and benzene in $AlPO_4$-5.[21,22,39] This suggests that the pentane isomers face lesser hindrance in their motion along the $AlPO_4$-5 channel as compared to the rigid molecules such as methane, ethane, and benzene. As expected, the VACF values for v_x and v_y show negative correlations, indicating the presence of confinement along these directions. In the carbon nanotube, VACF for v_z does not decay, leading to nondiffusive motion for both pentane isomers. Yet VACF values for the v_x and v_y components for isopentane and *n*-pentane show different behavior. For *n*-pentane, the oscillations in the VACF are observed up to $t = 1$ ps, while for isopentane the oscillations continue up to $t = 5$ ps (Figure 10b and e). This is due to the entrapment of the molecules in the potential minima near the channel wall (Figure 3c and d). In the case of isopentane, persistence of these oscillations for a longer period implies entrapment in the potential minima for longer duration. More frequent oscillations

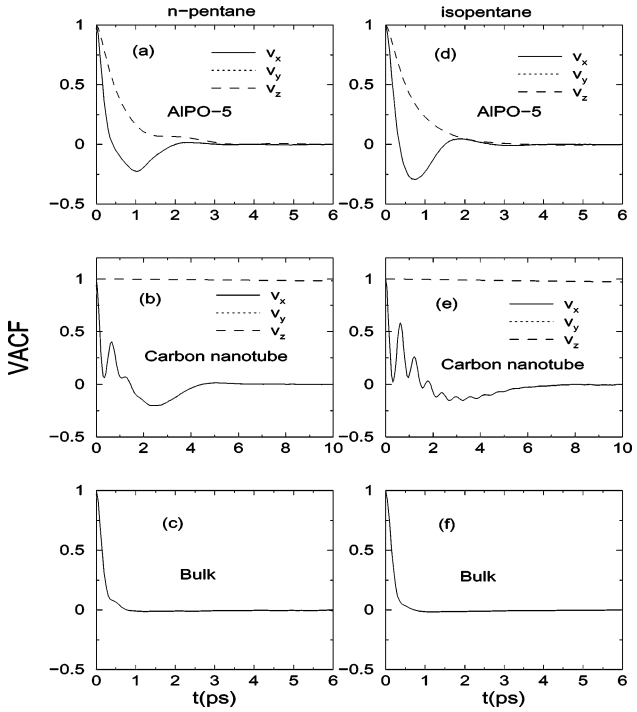

Figure 10. VACF of the center of mass velocity of *n*-pentane (a−c) and isopentane (d−f) in $AlPO_4$-5, carbon nanotube, and bulk, respectively, at $T = 200$ K.

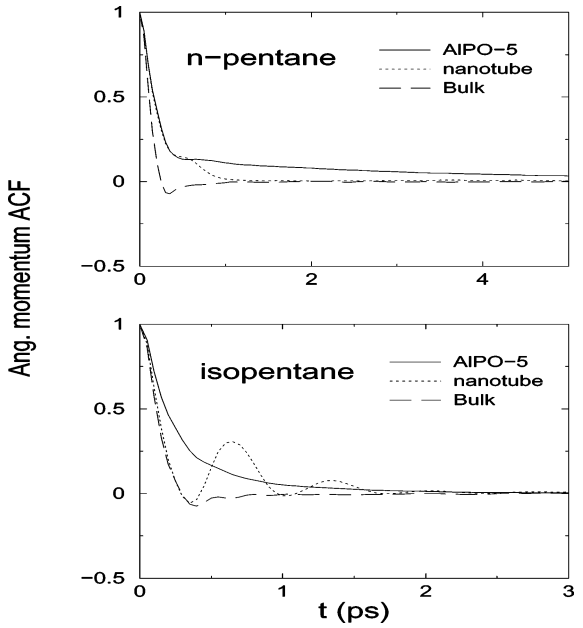

Figure 11. Angular momentum ACF of the angular momentum component parallel to the end-to-end vector, for pentane isomers in $AlPO_4$-5, carbon nanotube, and bulk at $T = 200$ K.

Table 6. Molecular Cross Section of the Pentane Isomers along with the γ Values for the Narrow (n) and Wide (w) Parts of the $AlPO_4$-5 Channel

isomer	d (Å)	σ_{gh} (Å)	γ_n	γ_w
n-pentane	0.855	3.217	0.80	0.71
isopentane	2.837	3.217	1.00	0.884

also indicate a deeper minimum which is consistent with results plotted in Figure 3d. This in turn gives rise to the reduced mobility of isopentane as compared to *n*-pentane in the nanotube (Figure 9). Figure 10c and f shows the total VACF for bulk *n*-pentane and isopentane. Comparison of VACF in bulk and in $AlPO_4$-5 shows that, in $AlPO_4$-5, the VACF for v_z shows almost a bulklike decay of correlations with an increased correlation time.

Finally, previous studies have shown that the self-diffusivity D is also a function of the parameter

$$\gamma = \frac{2^{7/6}\sigma_{gh} + d}{\sigma_w}$$

Here σ_w is the void cross section, and $2^{1/6}\sigma_{gh}$ is the distance at which the guest−zeolite interactions are optimum. The distance d is the cross-sectional diameter, as shown in Figure 11. For *n*-pentane, d is calculated for $\phi = 180°$, and in the case of isopentane, the projection is considered on a plane perpendicular to the $CH-CH_2$ bond. When γ is close to unity, it has been observed that the self-diffusivity is largest. We have therefore calculated γ for $AlPO_4$-5 in Table 6. The diameter of the carbon nanotube is wider than that of $AlPO_4$-5; therefore, γ values corresponding to pentane isomers inside the nanotube are lower (not listed). Because the void cross section for $AlPO_4$-5 varies, we have chosen the narrowest and the widest cross sections for σ_w. The relevant quantity is the narrowest void cross section, but the value of γ of the wider region also plays a role. The fact that isopentane has a higher diffusivity in $AlPO_4$-5 is partly due to the fact that γ_n value is closer to unity than *n*-pentane.

Rotational Motion. The angular momentum autocorrelation function (AMACF) for pentane isomers is plotted in Figure 11 for $AlPO_4$-5, carbon nanotube, and bulk. Here, angular momentum is calculated with respect to the center of mass of the pentane isomers. The AMACF is calculated for the component of angular momentum along the end-to-end vector of a molecule. The component of angular momentum perpendicular to the end-to-end vector does not decay to zero (not shown). In bulk, both *n*-pentane and isopentane show a small negative minimum, indicating a cage effect. *n*-Pentane in $AlPO_4$-5 and in the carbon nanotube does not show any cage effect but shows a long correlation time in $AlPO_4$-5, as compared to that in the carbon nanotube. In $AlPO_4$-5, isopentane shows a faster decay of AMACF than does *n*-pentane. In the carbon nanotube, isopentane shows positive peaks in AMACF, indicating oscillations in the angular momentum component along the end-to-end vector due to entrapment in the potential minima near the nanotube wall.

6. Conclusion

In the case of pentane isomers (*n*-pentane and isopentane) confined within one-dimensional channels of $AlPO_4$-5 and the carbon nanotube, the size and shape of the molecules significantly affect equilibrium static and dynamical properties.

Branching, as in isopentane, implies an increase in the cross-sectional area and a decrease in the end-to-end distance as compared to that in *n*-pentane, the linear alkane. This is reflected in the values of the parameter γ listed in Table 6. In $AlPO_4$-5, as a result, isopentane experiences a potential energy surface along the channel that is similar to other rigid molecules such as methane, ethane, and benzene; two maxima and two minima are seen per unit cell along the *c*-direction. In contrast, for

n-pentane, there are more frequent oscillations in the potential energy surface due to an increased length and a smaller cross-sectional area.

The self-diffusivity of isopentane is more than that of *n*-pentane in $AlPO_4$-5. One reason for this could be that the levitation parameter γ of isopentane is closer to unity in narrow as well as wider parts of the channel than is *n*-pentane. Further, in *n*-pentane, as seen from Figure 5, the end-to-end distance distribution (which has a one-to-one correspondence with the dihedral angle distribution) is different at different regions within the channel. This implies that the translational motion is coupled to the change in the dihedral angle. As any change in the latter is slow, the translational motion is necessarily slow. In the case of isopentane, the end-to-end distance distribution (Figure 5) does not change as it travels down the channel which enables it to diffuse faster. In the carbon nanotube, both of the pentane isomers are superdiffusive, but *n*-pentane has a higher mean squared displacement than isopentane. The VACFs suggest that for both isomers motion along the channel in $AlPO_4$-5 resembles that in bulk. This in turn makes self-diffusivity inside confinement an order of magnitude more than that in bulk. This is in contrast with the self-diffusion coefficient obtained for other molecules. This comparison is listed in Table 7. The value of self-diffusivity for *n*-pentane and isopentane in $AlPO_4$-5 is nearly an order of magnitude higher than that in bulk, while this is not the case for other rigid molecules.

All of the above results and conclusions are within the framework of the united atom model and the potential parameters used here.[40] If, instead, one is to use a potential with a site for each atom, this may result in a change in the cross-sectional area. This can alter the translational motion due to changes in γ. This can also alter rotational dynamics due to the changes in the radius of gyration and moment of inertia. Incorporation of lattice vibrations may cause reduction in D in $AlPO_4$-5, and in the case of the carbon nanotube value of the exponent α could be reduced by a small amount. Small changes in potential parameters may also alter the diffusivities significantly because γ values are close to unity.

Table 7. Self-Diffusion Coefficients for Different Molecules Obtained from MD

	D_{alpo} $\times 10^{-8}$ m^2/s	ρ_{alpo} g/cm^3	D_{bulk} $\times 10^{-8}$ m^2/s	ρ_{bulk} g/cm^3
methane	2.601	0.02	2.23	0.29
ethane	1.011	0.038	0.525	0.544
benzene	0.5088	0.049	0.31	0.864
n-pentane	2.7	0.0238	0.354	0.634
isopentane	3.33	0.0238	0.336	0.634

Acknowledgment. The authors wish to acknowledge the Department of Science and Technology, New Delhi for financial support. Financial support from the Department of Atomic Energy is also gratefully acknowledged. We also wish to thank the referees for comments.

JA0285868